Supplemental information

A Molecular Signature of Depression in the Amygdala

Etienne Sibille,[1,2,*] Yingjie Wang,[1] Jennifer Joeyen-Waldorf,[1] Chris Gaiteri,[1,2] Alexandre Surget,[4] Sunghee Oh,[3] Catherine Belzung,[4] George Tseng,[3] and David A Lewis[1,2]

[1]Department of Psychiatry, [2]Center for Neuroscience, [3]Department of Biostatistics, University of Pittsburgh, Pittsburgh, PA 15213, USA.

[4]U930 FRE CNRS 2448, INSERM and Université François Rabelais, 37200 Tours, France.

*Address correspondence to Etienne Sibille, Department of Psychiatry, University of Pittsburgh, 3811 O'Hara Street, BST W1643, Pittsburgh, PA 15213; sibilleel@upmc.edu (E-mail).

Table of contents

---

1. Detailed Material and Methods

Subjects

Brain samples were obtained during autopsies conducted at the Allegheny County Medical Examiner's Office following consent from the surviving next-of-kin. After careful examination of demographic, clinical and technical parameters, we selected a cohort of male depressed subjects and matched control samples.

For all subjects, consensus DSM-IV diagnoses of MDD were made by an independent committee of experienced clinical research scientists at a case conference utilizing information obtained from clinical records, toxicology exam and a standardized psychological autopsy (1). This latter incorporates a structured interview, conducted by a licensed clinical psychologist with family members of the index subject, to assess diagnosis, psychopathology, medical, social and family histories, as

well as history of substance abuse. A symptom score was calculated based on the presence at time of death (1= unequivocal yes; 0.5= unsure or subthreshold; 0= unequivocal no) of nine major depressive episode symptoms: depressed mood, anhedonia, appetite disturbance, sleep disturbance, psychomotor change, anergia, self-recrimination, diminished ability to concentrate or make decision, and suicidality.

We further focused on patients with familial depression, as these subjects in general display earlier onset of symptoms, more recurring episodes, shorter inter-episode duration, and suffer from more severe and incapacitating episodes than non-familial depressed patients (2). To determine familial MDD, the next-of-kin was asked about each 1st-degree family member and about the psychiatric history of other family members. This approach has the advantage of being prompt, efficient and appropriate for postmortem studies, but it also underestimates the presence of psychiatric illness in 1st-degree relatives (3). All MDD subjects had at least one 1st-degree relative with a history of MDD. The increased disease severity was supported by a longer average duration of illness in the familial depressed cohort compared to non-familial subjects collected under the same conditions in the same brain donation program (9±2 years versus 3±1 years; Mean±sem; t-Test, p=0.01).

Cases who did not commit suicide, died from natural causes, thus ruling out the possibility of accidental death as masked suicide. MDD subjects with co-morbid psychiatric disorders were excluded. Antidepressant drug exposure was assessed by clinical data from structured interviews, review of records and toxicology studies. Control subjects were paired to each case as closely as possible on age and freezer storage time. Control subjects did not have an Axis I psychiatric disorder, were antidepressant drug-free and died from natural or accidental causes other than suicide. The family histories of MDD in controls included one positive, nine negatives and six unknowns. Subjects with advanced disease stages (i.e., cancer, neurodegenerative disorders) were excluded. All cases and controls were white Caucasian and were selected for rapid modes of death and short agonal phases, to limit the influence of agonal factors on RNA quality and pH (4). All selected brains were analyzed for adequate brain pH (>6.4) and RNA integrity by optical density (OD≥ 1.6) and Agilent bioanalyzer analysis (Agilent Technologies, Palo Alto, CA; RIN expert scoring system ≥ 7) as previously described (5). Two pairs did not pass quality control in AMY, leaving 16 pairs in ACC and 14 pairs in AMY for the final analysis (Table 1). Rates of death by suicide, disease recurrence, evidence for antidepressant treatment at time of death, and alcohol dependence in MDD subjects are described in Table 1. Toxicological screens on peripheral fluids identified the presence of at least one antidepressant in 5 subjects, including four different tricyclics, one selective serotonin reuptake inhibitor and one weak dopamine reuptake inhibitor. Importantly, all antidepressant-treated subjects were currently depressed at time of death, suggesting either a lack of efficacy, suboptimal treatment or treatment-resistance in these subjects. All procedures were approved by the University of Pittsburgh's Institutional Review Board and Committee for Oversight of Research Involving the Dead.

Brain samples

Upon collection, coronal blocks through the rostral to caudal extent of the brain were cut in ~2 cm blocks and stored at -80C. The AMY is located ~2-3 cm caudal to the temporal pole. Tissue samples were dissected from 20µm section in the cryostat and stored in Trizol (Invitrogen, Carlsbad, CA). Sampling was adapted from (6) (Figure 1A in manuscript). The lateral and ventral borders were delimited by the white matter surrounding the AMY. The medial border was defined by the deep layer of the cortex along the medial edge of the temporal lobe. Finally, the dorsal border of the AMY was drawn along the lateral, basolateral and basomedian nuclei. In view of the heterogeneity of the AMY structure, we performed a pilot study to determine appropriate protocols for reliable and consistent dissection, and to assess the sample-to-sample variation in transcript levels within the rostral part of the AMY compared to more caudal samples. Rostral samples were reliably sub-dissected and

resulted in samples enriched in lateral, basolateral and basomedian nuclei tissue (7), while avoiding tissue dilution from the cortical and transitional amygdaloid nuclei that are more prominent in middle and caudal AMY. Rostral, middle and caudal AMY samples were processed on arrays. Results indicated that rostral sub-dissected samples displayed low intra-variability of RNA levels compared to more caudal samples (Figure 1A in manuscript). Accordingly, sampling proceeded on sub-dissected samples corresponding to rostral sections 1 and 2 in Figure 1A. This protocol enriches samples in nuclei of interest and increases the probability that signal differences will reflect subject differences rather than AMY rostral-caudal variability.

ACC samples containing all six cortical layers were harvested from coronal sections at the anatomical level corresponding to subgenual ACC (Brodman area 25), located in the third prefrontal cortex block along the rostral-caudal axis of the brain. A similar microarray pilot study revealed that, within a subject, very little variability in transcript levels was observed for most genes along 10mm of the rostral-caudal axis of the subgenual ACC (Figure 1B in manuscript), in agreement with the more homogeneous anatomical structure of this brain area compared to the AMY. Accordingly, sampling on all cases and controls occurred in the rostral part of the subgenual ACC, immediately caudal to the genu of the corpus callosum. Replicate samples were processed for 4 pairs in the AMY at 3-4 months interval from different RNA extractions obtained from the same subjects. A few white matter (WM) samples were obtained for analysis of cellular origin of transcripts (8). These samples were collected adjacent to the grey matter (GM) samples in ACC (n=7) and as an easily recognizable thin band located between the lateral and ventral borders of the amygdala (n=4).

WM/GM analysis

While subgroups of genes are expressed in cell type-specific manners, the majority of gene transcripts display relative enrichments across cell types, including neurons and glia. Here, we used array data from adjacent white matter (WM) samples to generate WM/GM ratios that are specific for each gene and brain region. We have shown that these ratios represent valid estimates of relative gene transcript enrichment from glia (WM/GM>1.5), neurons (WM/GM<-1.5) or both cellular population (-1.5<WM/GM<1.5) and that incorporating the use of these ratios into transcriptome analysis can provide wider views of overall patterns relating to glial and neuronal functions (8;9). Here, WM/GM ratios generated in control samples were used, although ratios generated in psychiatric subjects or treated mice were essentially identical, as Pearson correlation factors between control and all-samples ratios were greater than 0.99 (8).

Real-time quantitative real-time PCR (qPCR)

qPCR was performed as previously described (10;11). In brief, small PCR products (80-120 base-pairs) were amplified in quadruplets on an Opticon real-time PCR machine (Bio-Rad, Hercules, CA), using universal PCR conditions [65C to 59C touch-down, followed by 35 cycles (15" at 95C, 10" at 59C and 10" at 72C)]. 150 pg of cDNA was amplified in 20µl reactions [0.3X Sybr-green, 3mM $MgCl_2$, 200µM dNTPs, 200µM primers, 0.5 unit Platinum Taq DNA polymerase (Invitrogen, Carlsbad, CA)]. Primer-dimers were assessed by amplifying primers without cDNA. Primers were retained if they produced no primer-dimers or non-specific signal only after 35 cycles. Results were calculated as the geometric mean of the relative intensities compared to three internal control genes (actin, glyceraldehyde-3-phosphate dehydrogenase and cyclophilin).

Western Blot analysis

Proteins were isolated from phenol-ethanol supernatant obtained during the RNA isolation for array samples and re-suspended in urea/SDS buffer. 5µg of protein samples were resolved by SDS PAGE in 10% Tris/glycine gels and transferred to PVDF membrane. After 1 hour in Odyssey blocking buffer (LI-COR Biosciences, Lincoln, NE), the blots were incubated with primary antibodies [Rabbit anti-actin 1:10,000, Sigma #A2066, and mouse anti-cyclic nucleotide 3' phosphodiesterase (CNP); SMI-91R from Covance, Denver, PA] in Odyssey blocking buffer, followed by incubation with secondary

antibodies (IRDye® 800 anti-rabbit and 680 anti-mouse; LI-COR Biosciences). After extensive washing, the signals were simultaneously detected using the LI-COR Odyssey® Infrared imaging system. To compare protein content between different samples and to correct for any experimental variations that occur during sample processing on SDS PAGE and Western blots, CNP protein content was expressed relative to the actin content in the same sample. Paired samples were processed in quadruplicate on the same gel.

Gene coexpression networks *See Section #5*

2. FIGURE S1. AMY-ACC altered gene expression in MDD and qPCR validation

(a) Venn diagram of altered gene expression. 45% of these genes were upregulated and 55% downregulated in AMY, while ACC results displayed 60% and 40% up- and downregulated genes, respectively. Arrows indicate directional correlations between changes in transcript levels for genes identified in one area (origin of arrow) and changes for the same genes in the other area (end of arrow); $p<e^{-6}$ in both directions. Although the overlap in gene selection was limited, transcript changes in AMY and ACC significantly predicted similar trends for the same transcripts in the other area, suggesting coordinated changes across areas, despite variability in statistical thresholds.

(b) Technical validation of array results by independent qPCR measurements. Alr, Average Log_2 of (MDD/Control) expression ratio. (-DDCt) represent differences in PCR cycle thresholds between MDD and control samples, which are equivalent to Log_2 values of ratios (See also Table 3). Upregulated: *GRIN2B, DGKG, GABRA2, KCTD12, CALB1, DUSP4, GPNMB, ASPH, RAB27B*; Downregulated: *MOBP, CNP, EGR1, MBP, ENPP2, MAPK1, RPH3A*; Unchanged (*RAB27B*). For all but one (*GRIN2B*), qPCR and array results correlated highly (All genes, R=0.88, $p<5.e^{-6}$; y slope=1.07). Line indicates linear fit.

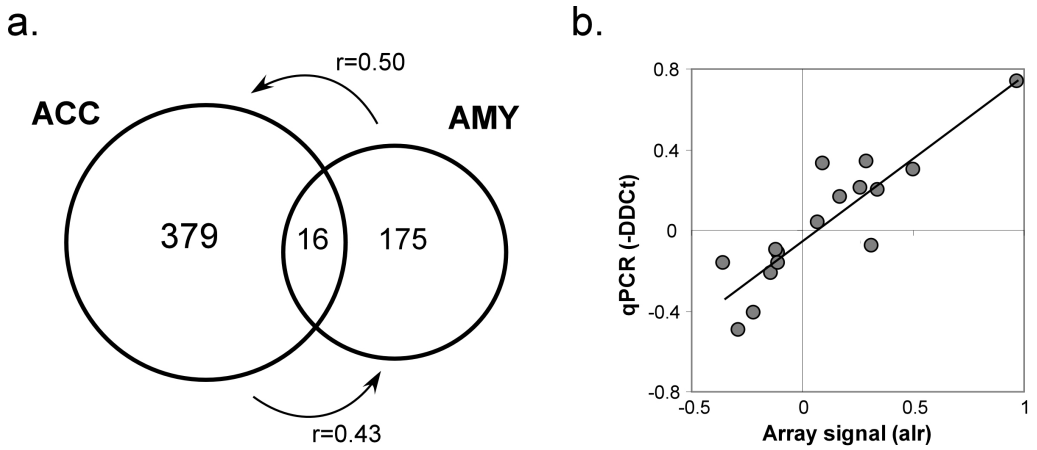

3. FIGURE S2. Positive correlation between the number of MDD symptoms and UCMS/MDD correspondence

See the following section in the manuscript: "AMY cross-species correlations of depression-related molecular changes identified a subgroup of human MDD subjects". The solid line indicates the linear fit for all 14 pairs in AMY (r=0.62; p=0.02). The dashed line indicates the linear fit after removing two subjects with 0 symptoms (r=0.51, p=0.09).Black squares indicate MDD^{UCMS} subjects.

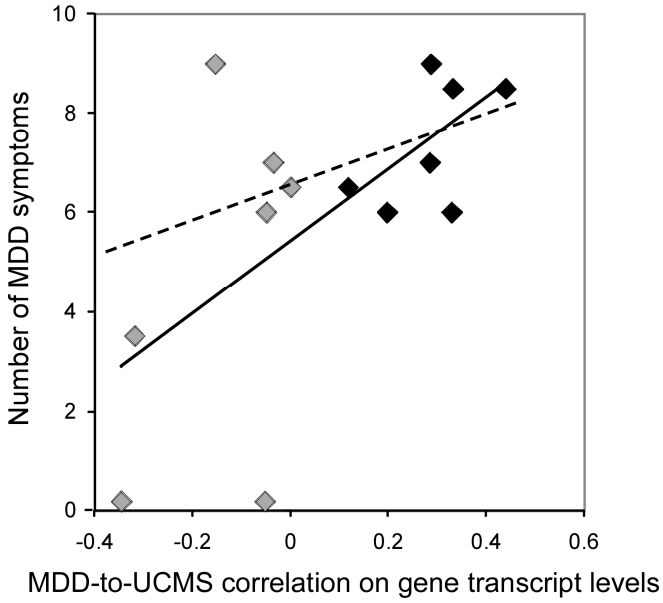

4. FIGURE S3. Antidepressant reversal of MDD conserved changes in the mouse UCMS model

32 genes displayed significant and highly similar changes in transcript levels in human depression and mouse UCMS (black dots). All changes were reversed in UCMS-exposed mice after treatments with an effective (fluoxetine; white squares) or a putative (Crf1R antagonist; grey diamonds) antidepressant treatments in UCMS-exposed mice. Values are from (12) and are described in Table 3.

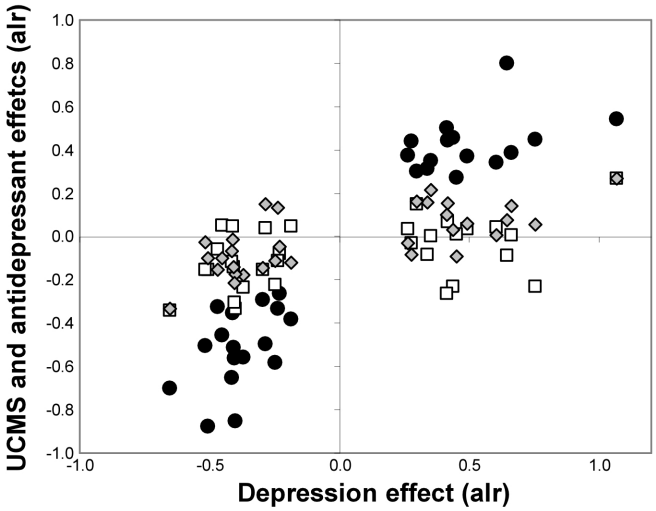

5. GENE COEXPRESSION NETWORKS (Methods & supporting findings)

Gene networks based on coexpression (i.e., correlated patterns of expression) appear to represent intrinsic attributes of cellular and neural systems that are helpful in identifying functionally-related genes (13). On the genomic scale, these gene interactions networks are clustered into functional modules (14) embedded within a generic scale-free structure (15) and this organization persists across species (16). Coexpression networks of genes built through Pearson correlation are broad yet reliable representation of gene interactions (13;17) and have successfully dissected canonical datasets into functional modules (18). We use the Pearson product-moment correlation coefficient to estimate pair-wise coexpression of our set of 32 genes in both mouse and humans. All analyses were performed using the boost graph library and custom MATLAB code. Network visualizations were created using Cytoscape.

Validity and robustness of experimentally derived networks

The sample sizes (n=6/group in mouse; 4 groups: Control, UCMS, UCMS+ fluoxetine, UCMS + CRF1R antagonist; n=14 pairs in human) ruled out the network creation through non-linear or information theoretic measures, which commonly require sample sizes that are an order of magnitude larger. Thus, to ensure that our coexpression links were reliable markers of gene interactions, we used clustering coefficient analysis (Step 1) and jackknife correlation (Step 2) to optimize our cut-off selection. Our goal was to use these techniques to optimize the biologically valid information in the network and to ensure an independent unbiased perspective on glial/neuronal gene regulation in depression.

Network Authentication Step 1: Network Validity

Clustering coefficients estimate the density of local connections in a network. They are calculated for each node in the network as the number of connections between neighboring nodes, divided by the total possible number of connections between all neighboring nodes. Clustering coefficients are a fundamental measure of network structure with wide applicability in brain networks (19). We used clustering coefficient as a signature of structural information in the network that was generated by a particular cutoff point, in a method based on Elo (2007). Maxima in the plot of clustering coefficient vs. cutoff represent an optimal ratio of the biological structure vs. noisy or spurious connections. In each case, we compared the clustering coefficients to degree-matched randomly selected networks (see representative plots in Figures S3-4). These plots showed maxima in the region of Pearson correlations of ~0.6-0.8 for all conditions in both species, indicating that using a Pearson correlation cutoff in this region would maximize the number of links which are representative of biological structure (20).

Network Authentication Step 2: Network Robustness

Pearson correlation is susceptible to outlying values. To prevent such occurrences from generating links in our networks, we used jackknife correlation in combination with an optimized cutoff threshold (Step 1) to optimally prune the network and maximize the biological signal. Figure S5 shows the common bimodal distributions of potential links that clearly segregated as either robust (i.e., right columns in graphs) or spurious (left columns in graphs) links in the human and mouse datasets. Links in our network were gathered from the most robust groups in jackknife histogram. Within each bin, links were selected in order of Pearson correlation value, beginning with the highest values, until the required network size was filled. Because of the hybrid link selection technique, actual Pearson correlation values of included links are substantially higher than cutoff values. A network size of 100 links will have: *1)* a cutoff value in the suggested range 0.65 (human) or 0.75 (mouse), *2)* will only be composed of robust links, and *3)* will be representative of glial-glial, neuronal-neuronal and neuronal-glial connectedness (See Fig 5). Results for networks with 100 bidirectional links are summarized in table S1. This rigorous criterion generated networks which are highly valid representation of underlying biological interactions.

Table S1. Pearson cutoff values are selected by monitoring increased clustering coefficients of experimental networks vs. controls (rows 1 and 3). Genes above the cutoff value are then selected in order of their robustness in jackknife correlation. Combining these techniques naturally leads to the selection of genes with a higher correlation than the baseline cutoff (row 2).

	Human		Mouse			
	Control	**MDD**	**Control**	**UCMS**	**Fluoxetine**	**Crf1R atg**
Pearson cutoff in jackknife correlation	0.65	0.65	0.75	0.75	0.75	0.75
Average Pearson correlation value of links	0.77	0.76	0.93	0.93	0.88	0.9
% increase of clustering coefficient vs Random network	60	110	95	41	76	77

6. REFERENCES

1. Glantz LA, Lewis DA: Reduction of synaptophysin immunoreactivity in the prefrontal cortex of subjects with schizophrenia. Regional and diagnostic specificity. Arch Gen Psychiatry 1997; 54:660-669
2. Fava M, Kendler KS: Major depressive disorder. Neuron 2000; 28:335-341
3. Andreasen NC, Endicott J, Spitzer RL, Winokur G: The family history method using diagnostic criteria. Reliability and validity. Arch Gen Psychiatry 1977; 34:1229-1235
4. Tomita H, Vawter MP, Walsh DM, Evans SJ, Choudary PV, Li J, Overman KM, Atz ME, Myers RM, Jones EG, Watson SJ, Akil H, Bunney WE, Jr.: Effect of agonal and postmortem factors on gene expression profile: quality control in microarray analyses of postmortem human brain. Biol Psychiatry 2004; 55:346-352
5. Eggan SM, Hashimoto T, Lewis DA: Reduced cortical cannabinoid 1 receptor messenger RNA and protein expression in schizophrenia. Arch Gen Psychiatry 2008; 65:772-784
6. Hamidi M, Drevets WC, Price JL: Glial reduction in amygdala in major depressive disorder is due to oligodendrocytes. Biol Psychiatry 2004; 55:563-569
7. De Olmos JS: Amygdala in The human nervous system Edited by Paxinos G, Mai JK. San Diego, CA, Elsevier, 2004, pp 739-868
8. Sibille E, Arango V, Joeyen-Waldorf J, Wang Y, Leman S, Surget A, Belzung C, Mann JJ, Lewis DA: Large-scale estimates of cellular origins of mRNAs: Enhancing the yield of transcriptome analyses. J Neurosci Methods 2008; 167:198-206
9. Erraji-BenChekroun L, Underwood MD, Arango V, Galfalvy HC, Pavlidis P, Smyrniotopoulos P, Mann JJ, Sibille E: Molecular aging in human prefrontal cortex is selective and continuous throughout adult life. Biological Psychiatry 2005; 57:549-558
10. Galfalvy HC, Erraji-Benchekroun L, Smyrniotopoulos P, Pavlidis P, Ellis SP, Mann JJ, Sibille E, Arango V: Sex genes for genomic analysis in human brain: internal controls for comparison of probe level data extraction. BMC Bioinformatics 2003; 4:37
11. Sibille E, Arango V, Galfalvy HC, Pavlidis P, Erraji-BenChekroun L, Ellis SP, Mann JJ: Gene expression profiling of depression and suicide in human prefrontal cortex. Neuropsychopharmacology 2004; 29:351-361
12. Surget A, Wang Y, Leman S, Ibarguen-Vargas Y, edgar NM, Griebel G, Belzung C, Sibille E: Corticolimbic transcriptome changes are state-dependent and region-specific in a rodent model of depression and of antidepressant reversal. Neuropsychopharmacology 2008; Advanced on-line:1-18
13. Lee HK, Hsu AK, Sajdak J, Qin J, Pavlidis P: Coexpression analysis of human genes across many microarray data sets. Genome Research 2003; 14:1085-1094
14. Zhang B, Horvath S: A general framework for weighted gene co-expression network analysis. Stat Appl Genet Mol Biol 2005; 4:Article17
15. Agrawal H: Extreme self-organization in networks constructed from gene expression data. Phys Rev Lett 2002; 89:268702
16. Bergmann S, Ihmels J, Barkai N: Similarities and differences in genome-wide expression data of six organisms. PLoS Biol 2004; 2:E9
17. Eisen MB, Spellman PT, Brown PO, Botstein D: Cluster analysis and display of genome-wide expression patterns. Proc Natl Acad Sci U S A 1998; 95:14863-14868
18. Carlson MR, Zhang B, Fang Z, Mischel PS, Horvath S, Nelson SF: Gene connectivity, function, and sequence conservation: predictions from modular yeast co-expression networks. BMC Genomics 2006; 7:40
19. Sporns O, Chialvo DR, Kaiser M, Hilgetag CC: Organization, development and function of complex brain networks. Trends Cogn Sci 2004; 8:418-425
20. Elo LL, Jarvenpaa H, Oresic M, Lahesmaa R, Aittokallio T: Systematic construction of gene coexpression networks with applications to human T helper cell differentiation process. Bioinformatics 2007; 23:2096-2103